Article

Surface Activity and Electrochemical Behavior of Some Thiazine Cationic Surfactants and Their Efficiency as Corrosion Inhibitors for Carbon Steel in a Sour Environment

Mohamed A. Moselhy, Elsayed Gamal Zaki,* Samir Abd El Hady Abd El-Maksoud, and Mohamed A. Migahed

Read Online

ACCESS | 📊 Metrics & More | 📰 Article Recommendations

ABSTRACT: The inhibition efficiency of cationic surfactants such as 1-ethyl-4H-benzo[d][1,3]thiazin-1-ium bromide (BTB) and N-ethyl-N,N-dioctyloctan-1-aminium bromide (DAB) for X-65 type carbon steel in oil well formation water under a H_2S environment has been studied using potentiodynamic polarization and electrochemical impedance spectroscopy measurements. Fourier transform infrared and nuclear magnetic resonance spectroscopy techniques were used to confirm the chemical structures of BTB and DAB. The novelty of this work lies in modifying the long chains in the inhibitor, which leads to high efficiency. These surfactants act as good inhibitors, which inhibit both cathodic and anodic routes by adsorption on the electrode surface, which is compatible with the critical micelle concentration parameters, together with a slight positive change in the corrosion potential (E_{corr}). The IE% reached 93.4% for compound BTB and 84% for compound DAB at 250 ppm. The equivalent circuit was used to analyze the model of the corrosion inhibition process. The atomic force microscopy image shows the morphology of the adsorbed layer formed on the steel alloy. Finally, a suitable inhibition mechanism was proposed.
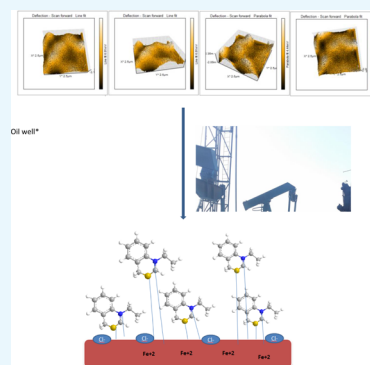
1. INTRODUCTION

In petroleum fields, carbon steel has been used in many applications.[1,2] These applications, for the most part, incite genuine destructive impacts on types of gear, tubes, and pipelines made of iron and its alloys.[3,4] Subsequently, the counteractive action of metals used in the petroleum field and modern applications from consumption is indispensable, which must be managed, particularly in corrosive media. Cationic surfactants as a branch of surfactants play a vital role in many industrial processes such as food processing, oil recovery, and in petroleum additives like corrosion inhibitors.[5−17]

The inhibition efficacy is directly proportional to the inhibitor concentration and contact time with the metal surface. Many industrial processes generate gases like carbon dioxide, ammonia, and hydrogen disulfide. This latter gas contains sulfide ions, which react with many heavy metals. H_2S is a pale gas with an offensive odor suggestive of rotten eggs. It is a weak reducing acid and is readily soluble in water with subsequent ionic dissociation.

H_2S forms black metallic sulfide suspensions and/or deposits induced by corrosion. H_2S enters the matrix of many alloys, resulting in brittleness in these alloys and stress corrosion cracking miscarriage particularly due to the high-strength steel.[18−26] The novelty of this work lies in modifying the long chains in inhibitors, which leads to high efficiency. The current research aims to prepare novel cationic surfactants, 1-ethyl-4H-benzo[d][1,3]thiazin-1-ium bromide (BTB) and N-ethyl-N,N-dioctyloctan-1-aminium bromide (DAB), and evaluate their efficiency as corrosion inhibitors for X-65 type carbon steel in oil well formation water in a hydrogen sulfide environment using different techniques.

2. RESULTS AND DISCUSSION

2.1. Potentiodynamic Polarization Study. Existence of hydrogen sulfide in the solution forms ferrous sulfide. The high concentration of gas results in failure of the protective layer as shown in eq 2. Corrosion potential (E_{corr}), corrosion current density (i_{corr}), cathodic and anodic Tafel slopes (βc and βa), and polarization resistance (R_p) as electrochemical parameters were calculated.

From the polarization curves shown in Figure 1a,b, it was observed that i_{corr} reduced with increasing dose of compounds BTB and DAB compared to the blank. The following equations
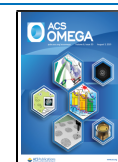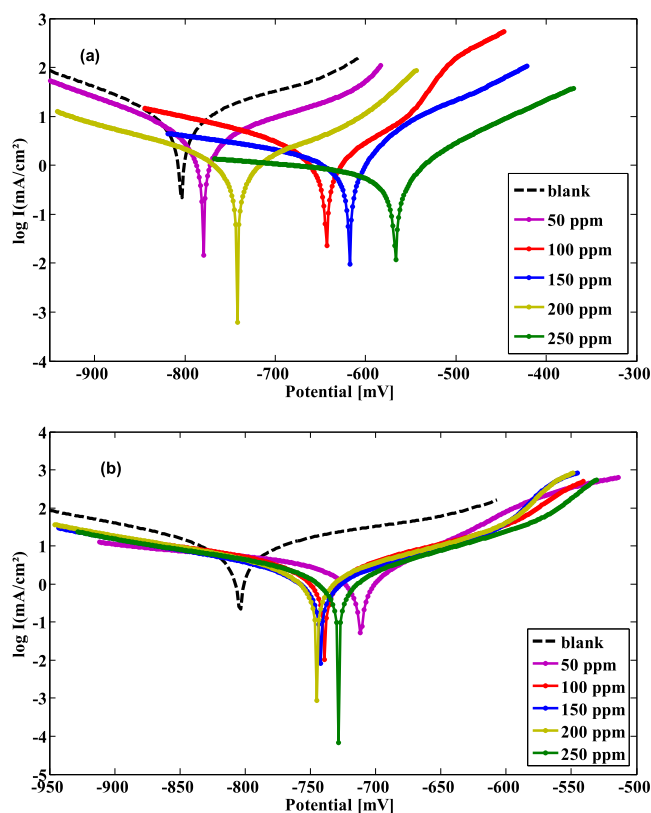
Figure 1. Polarization plots of the steel electrode in formation water containing various concentrations of (a) BTB and (b) DAB inhibitors.

are used for calculating the degree of surface coverage (θ) and the inhibition efficacy ratio ($\eta\%$):

$$\theta = 1 - \frac{i}{i_0} \tag{1}$$

$$\eta\% = \left(1 - \frac{i}{i_0}\right) \tag{2}$$

where i_0 and i are the corrosion current densities in the absence and presence of the inhibitor, respectively.

A good evaluation of the cathodic curve showed that the Tafel lines became more negative and so certain opportunities for both anodic and cathodic cycles, individually, comparative with the clear. This implies that the chose intensifies goes about as a blended kind inhibitor, that is, empowering block of both anodic and cathodic release responses. We notice that the
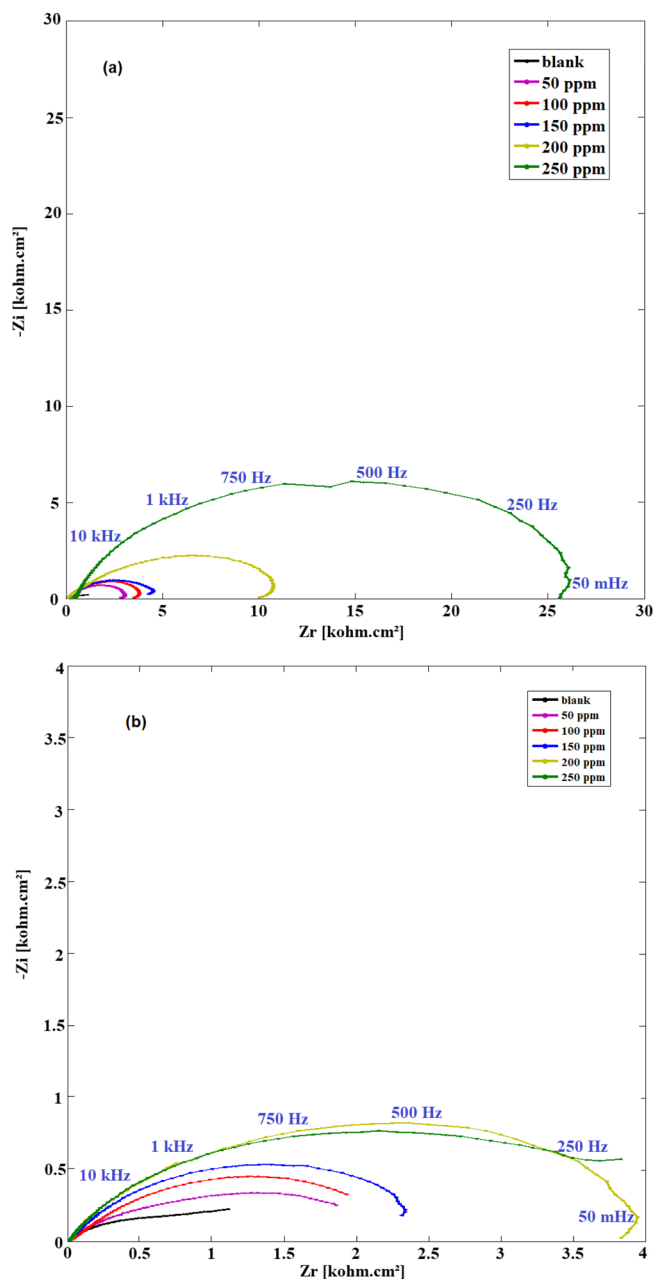

Figure 2. Nyquist plots for the carbon steel electrode in formation water with and without various concentrations of (a) BTB and (b) DAB inhibitors.

Table 1. Corrosion Parameters Obtained from Polarization Curves for BTB and DAB Inhibitors

| inhibitor	concentration (ppm)	βa (mV dec^{-1})	βc (mV dec^{-1})	E_{corr} (mV vs SCE)	i_{corr} (μA cm^{-2})	θ	IE%
blank	000	193.7	−150.9	−804.2	9.312		
BTB	50	109.4	−142.1	−779.7	3.433	0.6313	63.13
	100	79.7	−156.9	−643.5	2.405	0.7417	74.17
	150	103.9	−192.7	−617.6	1.357	0.8542	85.42
	200	104.9	−153.4	−741.8	0.855	0.9081	90.81
	250	103.4	−193.3	−567	0.638	0.9314	93.14
DAB	50	75.8	−139	−711.4	2.9143	0.6870	68.70
	100	110.6	−124.5	−739	2.87	0.6917	69.17
	150	109.1	−159.1	−745.5	1.942	0.7914	79.14
	200	102.3	−169.7	−728.5	1.854	0.8009	80.09
	250	71.2	−155.7	−742.1	1.499	0.8390	83.90
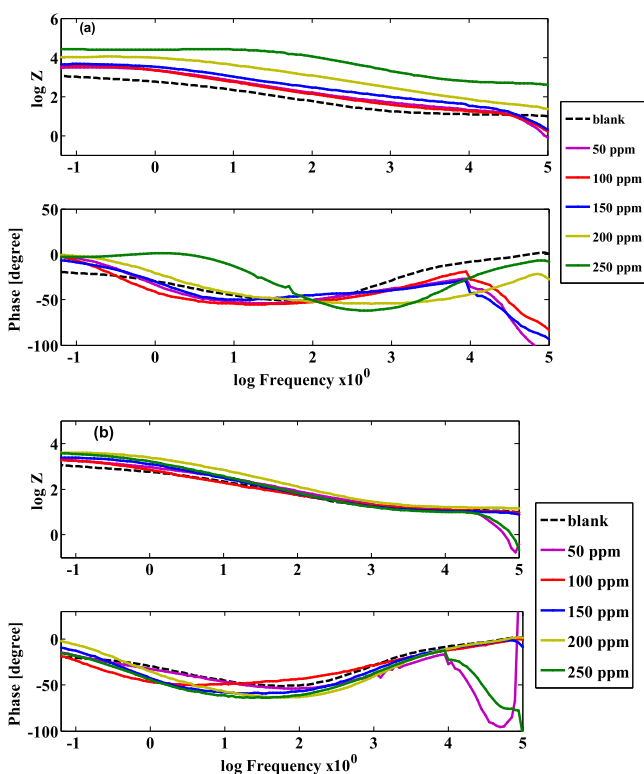
Figure 3. Bode plots for the carbon steel electrode in formation water with and without various concentrations of (a) BTB and (b) DAB inhibitors.

slopes of both the anodic and cathodic Tafel shapes were the same. This means that the selected inhibitor does not affect the metal dissolution mechanism. i_{corr} was reduced with the increase in the dose.[27] The obtained results summarized in Table 1 indicate that the i values are significantly lower in the presence of corrosion inhibitors compared to blank solutions. The corrosion current density decreases. The data obtained from the polarization curves are plotted and listed in Table 1.

From the polarization curves, it is observed that $\eta\%$ of the compound BTB is more than that of the accumulated DAB.

This could be attributed to the $p\pi-d\pi$ connections between the inhibitor particles and the empty orbital of Fe.[28−30]

2.2. Electrochemical Impedance Spectroscopy (EIS). Figures 2 and 3 show the Nyquist and bode plots of carbon steel immersed in the solution (blank) in the absence and presence of BTB and DAB, respectively.

It is clear that there is a depressed capacitive loop along the x-axis. The size of the loop increased on increasing the inhibitor concentration. This behavior indicated that the corrosion process was controlled by the polarization resistance according to the following equation[23]

$$R_p = R_s + R_f + R_{ct} \tag{3}$$

Figure 4 shows the equivalent circuit R_s, film resistance R_f, charge-transfer resistance R_{ct}, constant phase elements CPE_f and CPE_{cd} as obtained from the EIS analyzer program, and the obtained impedance data can be explained according to the following equation[24]

$$Z_{cpe} = 1/Y_0 \, (jw)^n \tag{4}$$

where Y_0 represents the admittance, $j = -1$, and w is the angular frequency.

It is obvious from Table 2 that both C_{dl} and C_f decrease with an increase in the concentration of BTB and DAB.

This is evidence for the adsorption of the inhibitor molecules on the carbon steel surface, forming the required protective layer. According to the following two equations[31]

$$C_{dl} = \sum \sum^0 Se/d \tag{5}$$

$$C_f = F^2 Se/4RT \tag{6}$$

where d is the thickness of the adsorbed layer, Se is the electrode surface exposed to the aggressive solution, $\sum^0$ is the permittivity of the vacuum, $\sum$ is the local dielectric constant, and F is Faraday's constant.

Figure 3a,b shows that the phase angle increased with increasing inhibitor concentration for carbon steel (CS) immersed in media of an corrosive environment in the presence of various doses of the two chemicals used (BTB and DAB), which shows different trends compared to the blank
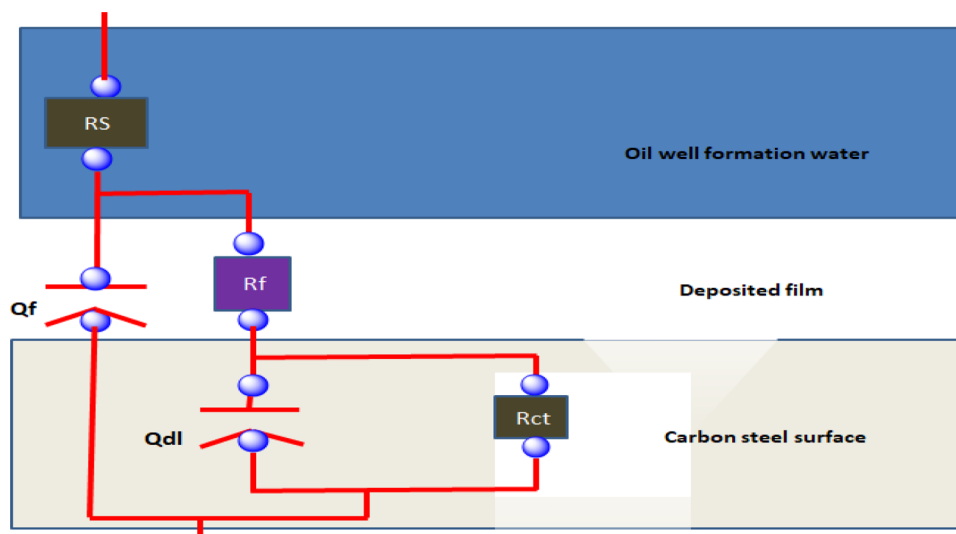

Figure 4. Equivalent circuit model for the impedance data.

Table 2. Impedance Parameters Obtained from the EIS Curves for BTB and DAB Inhibitors

| inhibitor	concentration (ppm)	R_f (Ω)	Q_F (μF/cm²)	n_1	Q_{dll} (μF/cm²)	R_{ct} (KΩ/cm²)	n_2	θ	IE %
BTB	0	52.6 + 2	132.1 + 1.1	0.87 + 0.02	538.1	1.659 + 0.10	0.83 + 0.05		
	50	128.9 + 3	87.3 + 0.9	0.92 + 0.03	40.90	3.112 + 0.017	0.88 + 0.03	0.4669	46.69
	100	286.2 + 5	63.7 + 0.8	0.94 + 0.01	56.45	3.995 + 0.015	0.91 + 0.02	0.5847	58.47
	150	423.3 + 6	52.6 + 0.7	0.96 + 0.04	23.41	4.905 + 0.014	0.92 + 0.01	0.6617	66.17
	200	560.7 + 4	46.8 + 0.8	0.97 + 0.01	4.641	11.03 + 0.013	0.93 + .01	0.8495	84.95
	250	592.5 + 7	37.2 + 0.4	0.98 + 0.01	143.9	25.51 + 0.012	0.93 + 0.01	0.9349	93.49
DAB	50	117.8 + 2	76.8 + 0.8	0.88 + 0.03	228.8	2.474 + 0.016	0.85 + 0.05	0.3294	32.94
	100	187.5 + 4	58.1 + 0.6	0.89 + 0.01	315.5	2.541 + 0.017	0.87 + 0.07	0.3471	34.71
	150	238.1 + 6	49.6 + 0.5	0.90 + 0.04	109.3	2.609 + 0.013	0.89 + 0.02	0.3641	36.41
	200	302.7 + 7	39.5 + 0.4	0.92 + 0.02	43.77	4.096 + 0.012	0.90 + 0.01	0.5949	59.49
	250	327.9 + 8	27.4 + 0.3	0.92 + 0.01	100.1	4.446 + 0.011	0.90 + 0.01	0.6268	62.68
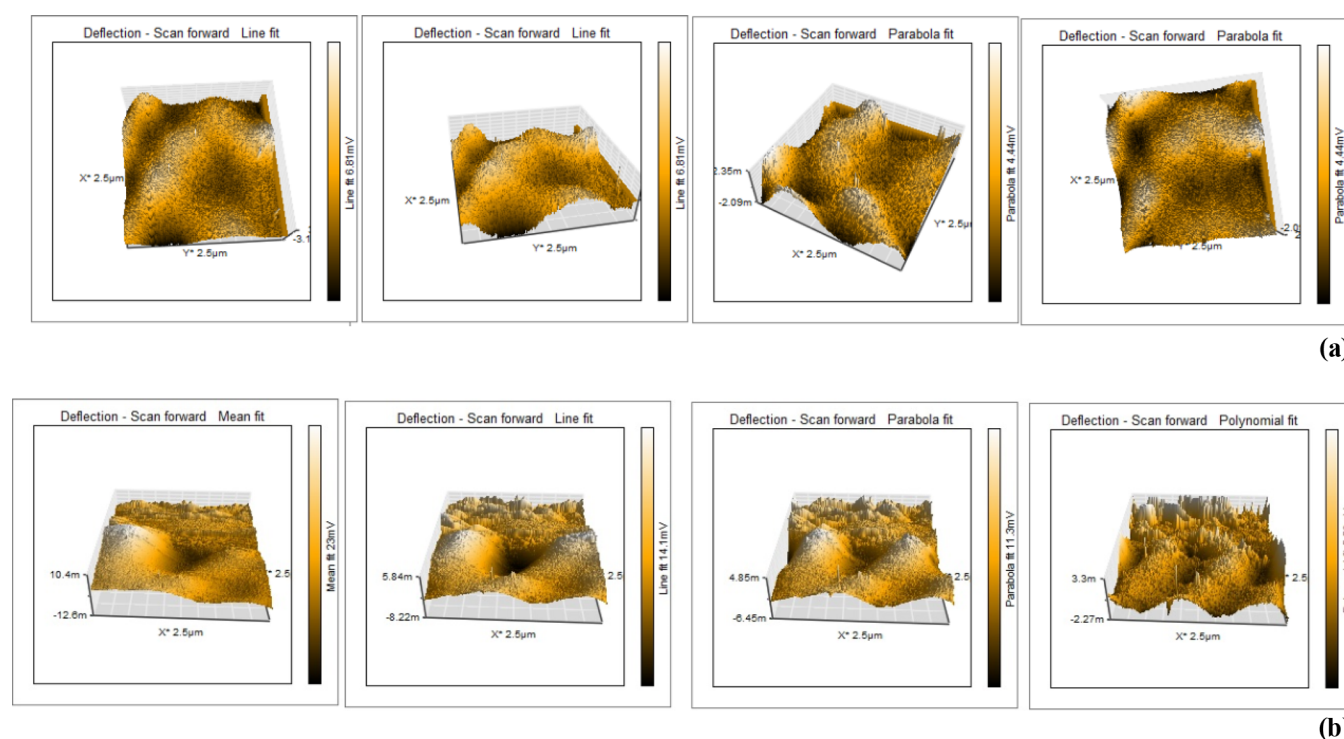
Figure 5. AFM images of (a) the CS samples before immersion in oil well formation water alone (blank) and (b) CS surface immersion in oil well formation water for 1 day using 250 ppm of the compound BTB.

Table 3. AFM Measurements of CS Samples in the Presence and Absence of Doses (250 ppm) of Compound BTB in Deep Oil Well Formation Water for 7 Days at 298 K

sample	average roughness (Ra), nm	RMS roughness (Rq), nm
CS alloy surface immersed in deep oil well formation water in the absence of inhibitor molecules	260.4	318.2
CS alloy surface immersed in 0.1 oil well formation water after immersion in 250 ppm of BTB	95.3	112.6

solution. It is clear from the variation of log Z with F that the impedance values increase with increasing concentration. Also, it is clear that the variation of phase angle increases with the increasing inhibitor concentration. The shift of the phase angle from the value of 90° is evidence for the deviation from the ideal capacitive behavior. This behavior confirms the obtained data from Nyquist plots. The inhibitive ability, which is reflected by η%, markedly improved as the inhibitor concentration increased.[32−34]

2.3. Atomic Force Microscopy (AFM) Surface Study. An atomic force microscope is an instrument used to discriminate the shallow design of geography since it is equipped for giving pictures. AFM investigated the extent of inhibition of CS after immersion in a destructive acid solution.[35] Figure 5 shows the 3D AFM morphologies for the dissolution of CS in a corrosive solution of deep oil formation water in the absence and the presence of 250 ppm of the compound. The root mean square (RMS) of unpleasantness (Rq) is the normal deviance that decides the normal lines and normal harshness (Ra), clarifying the mean deviance of all harshness pictures. The AFM image of CS in a destructive medium alone in oil well formation water shows extraordinary consumption and more harshness. Interestingly, a lesser number of sites attack when using the compounds because of the shape of the adsorbing films that shield the CS surface from its current circumstance. The %IE obtained from electrochemical measurements upheld and was consistent
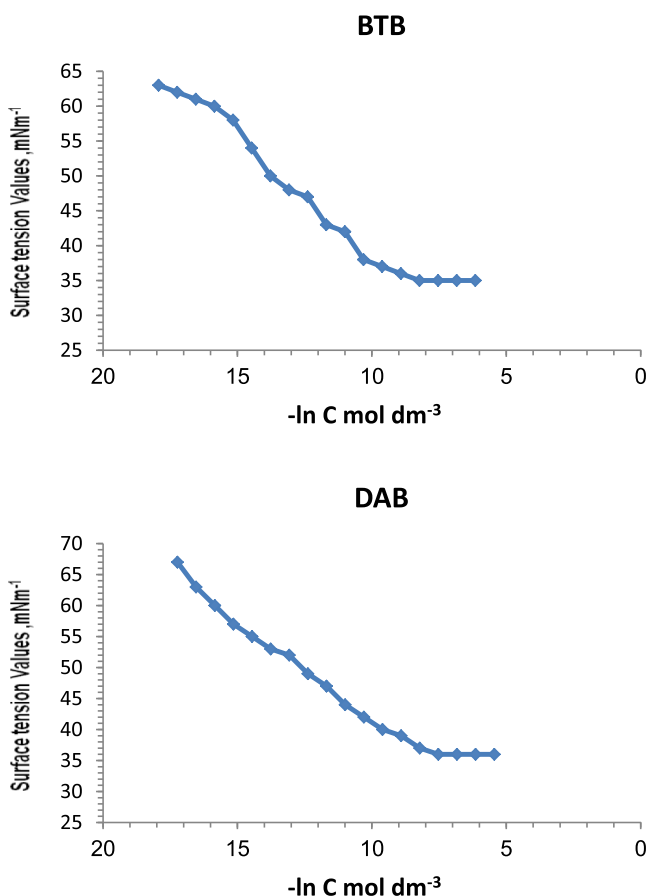
BTB

DAB

Figure 6. Surface tension vs log C of compound BTB and DAB.

Table 5. Standard Free Energy of Micellization (ΔG^0_{mic}) and Standard Free Energy of Adsorption (ΔG^0_{ads})

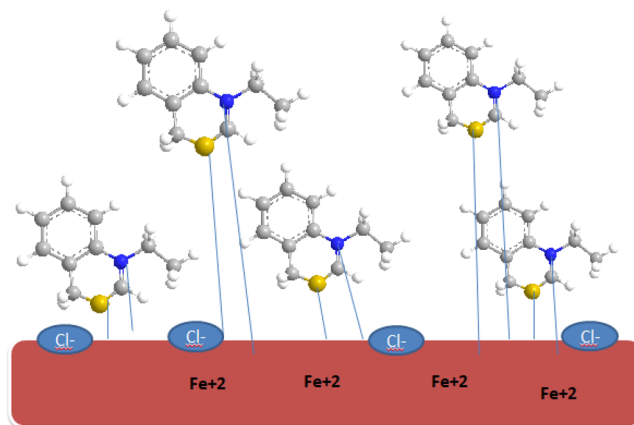| inhibitor	free energy of micellization ΔG^0_{mic} (kJ mol^{-1})	free energy of adsorption ΔG^0_{ads} (kJ mol^{-1})
BTB	−18.13	−21.96
DAB	−20.9	−23.7

Figure 7. Corrosion inhibition mechanism of BTB.

This demonstrates that compound BTB has the most grounded adsorption layer on the CS surface and hence the greatest inhibition efficiency, which stresses that the inhibition efficacies of the integrated compound expansion in the accompanying request as anticipated by the various methods: Tafel polarization and EIS . Using the following equation, it was found that the standard free energy of micellization (ΔG^0_{mic}) of compound DAB was lower than that of compound BTB for the synthesized surfactants:

$$\Delta G^0_{mic} = RT\ln CMC \tag{7}$$

The free energy of adsorption standard (ΔG^0 ads) for the synthesized surfactants is shown in the following equation:

$$\Delta G^0_{ads} = -RT\ln K_{ads} \tag{8}$$

where K_{ads} is the adsorption equilibrium constant. These results reveal that BTB with a longer alkyl chain possesses stronger adsorption affinity onto the CS surface and thus exhibits a better inhibition behavior.[36]

2.5. Inhibition Mechanism of Surfactants. The inhibition effecting for the deterioration of CS in oil well formation water was explored utilizing the examined surfactants BTB and DAB. The interference cycle depends on numerous factors like focus, the quantity of active areas and their charge densities, atomic mass, and their stability in their environments.[37] In fact, the heterogeneity of surfactants with uncommon nucleophilicity, electrons and charge of heteroatoms (N, O, and S particles) will in general limit the utilization of the metal surface. The barrier depends upon the adsorption of the surfactants on the CS surface and hindering their active centers.[38] Figure 7 shows the advancement of the

with the deliberate harshness information. Table 3 shows the understanding of Ra and Rq esteems. In an overall perspective on harshness, the metal surface is smoothed and turns out to be delicate because of the presence of an emphatically adsorbed layer through the dynamic community position of the inhibitor.

2.4. Surface Tension Characteristics. The critical micelle concentration of the prepared compounds was determined at different concentrations by adjustment of the slope of the plotted information of external strain surface tension (γ) versus the natural logarithm of the solute molar concentration, ln concentration, as presented in Figure 6. Table 4 summarizes the surface tension characteristics.

The critical micelle concentration (CMC) is a vital factor which turns out to be thermodynamically positive for surfactant atoms with respect to the structure totals (micelles) to limit the collaboration of either their head gatherings or their tail bunches with the dissolvable condition. Table 5 summarizes the standard free energy of micellization (ΔG^0_{mic}) and adsorption (ΔG^0_{ads}), which showed that compound BTB favors micellization rather than adsorption compared to inhibitor DAB with imported benzene ring and long chains.

Table 4. Surface Tension Characteristics of BTB and DAB

inhibitor	CMC, mole/dm^3	γ_{cmc}, mN/m	Γ max $\times 10^{-7}$, mol/m^2	Amin, n m^2	Π CMC	ΔG^0_{mic}, kJmol^{-1}	ΔG^0_{ads}, kJ mol^{-1}
BTB	7.47×10^{-4}	36	9.48×10^{-11}	175	36.5	−18.13	−21.96
DAB	2.49×10^{-4}	33	1.38×10^{-10}	119.5	39.3	−20.9	−23.7

Table 6. Physical Properties of the Testing Solution

total dissolved solids (TDS)	9650 mg/L	density@60 F	1.06 g/mL
salinity (as NaCl)	95,556 mg/L	specific gravity	1.06
alkalinity (as $CaCO_3$)	320 mg/L	pH@25 °C	6.8
total hardness (as $CaCO_3$)	14,455 mg/L	conductivity	12.02×10^{-2} mhos/cm@21.6 °C
		resistivity	0.0832 Ohm m@21.6 °C

Table 7. Chemical Composition of the Testing Solution

cation	mg/L	meq/L	anion	mg/L	meq/L
lithium	48.9	7.056	fluoride	76.71	4.038
sodium	30760.9	1337.485	chloride	57912.87	1631.405
ammonium	186.85	10.357	bromide	252.62	3.163
potassium	945.24	24.179	nitrate	38.17	0.616
magnesium	947.95	78.007	nitrite	1.84	0.040
calcium	4225.67	210.861	phosphate	nil	nil
strontium	78.08	1.783	sulfate	640.54	13.342
barium	1.30	0.019	hydroxide	nil	nil
iron	nil	nil	carbonate	nil	nil
copper	nil	nil	bicarbonate	390.40	6.399

Scheme 1. Synthesis of the Cationic Surfactant (BTB)

1-ethyl-4*H*-benzo[*d*][1,3]thiazin-1-ium
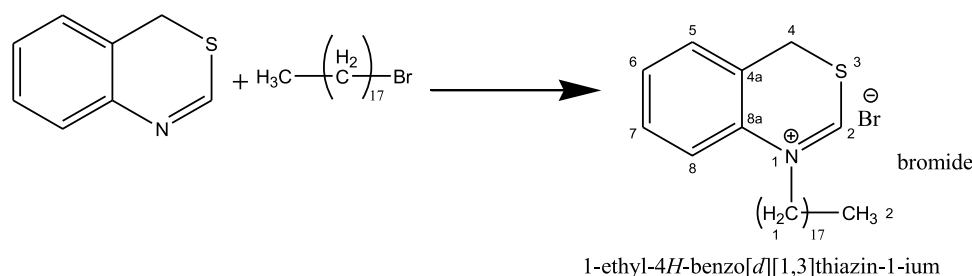
Scheme 2. Synthesis of the Cationic Surfactant (DAB)

N-ethyl-*N*,*N*-dioctyloctan-1-aminium
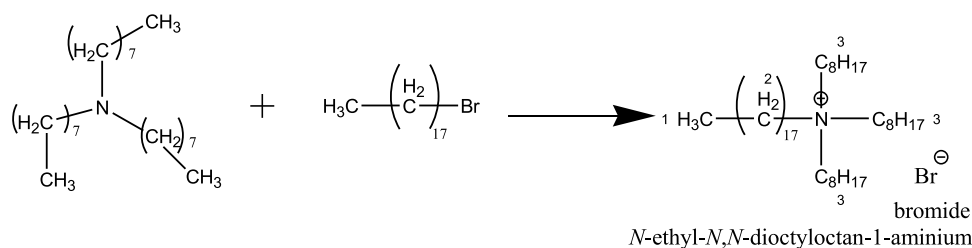
fused surfactant compounds containing heads and tails. The head hordes of the surfactants (polar part) were in rich electronically unique utilitarian social affairs, which share in the adsorption association with unfilled d-orbitals of the CS, through the relocation of adsorbed water particles from the CS by heteromolecules that can give the electron chemisorption bonding.[39]

The hydrophobicity chain (tail) of the surfactant causes the relocation of the surfactants from the game plan mass to associate, and these hydrophobic tails work as a resistance film to keep the metal away from reacting with its present situation. The adsorption collaboration depends on the tendency of the CS toward electron densities that work with better surface coverage.[40]

3. EXPERIMENTAL SECTION

3.1. Chemical Structure of the X-65 Type CS Electrode. An unused petroleum pipeline was cut into X-65 type CS specimens. The chemical composition (weight %) of

the CS electrode was carbon, 0.09; silicon, 0.22; Mn, 1.52; P, 0.01; S, 0.05; Ni, 0.04; Cr, 0.02; Mo, 0.004; vanadium, 0.002; copper, 0.02; and aluminum, 0.04; and the rest was Fe.

3.2. Deep Oil Well Formation Water. The reservoir rock contains deep oil well formation water. This water contains different organic and inorganic salts. The elements present are Na, Ca, Mg, Cl, HCO_3, and SO_4. The chemical composition of this water and its physical properties are summarized in Tables 6 and 7.

3.3. Testing Solution. The testing solution is the oil well formation water containing the abovementioned specific chemical compositions. The reaction of sodium sulfide (3.53 mg L^{-1}) with acetic acid (1.7 mg L^{-1}) generates hydrogen sulfide gas. This is called the simulation solution, which is similar to actual media in oil wells. This work facilitates preparation inhibitors as semi-industrial or industrial of inhibitors.

3.4. Synthesis of the Inhibitors. The cationic surfactant BTB based on benzothiazole was prepared as illustrated in
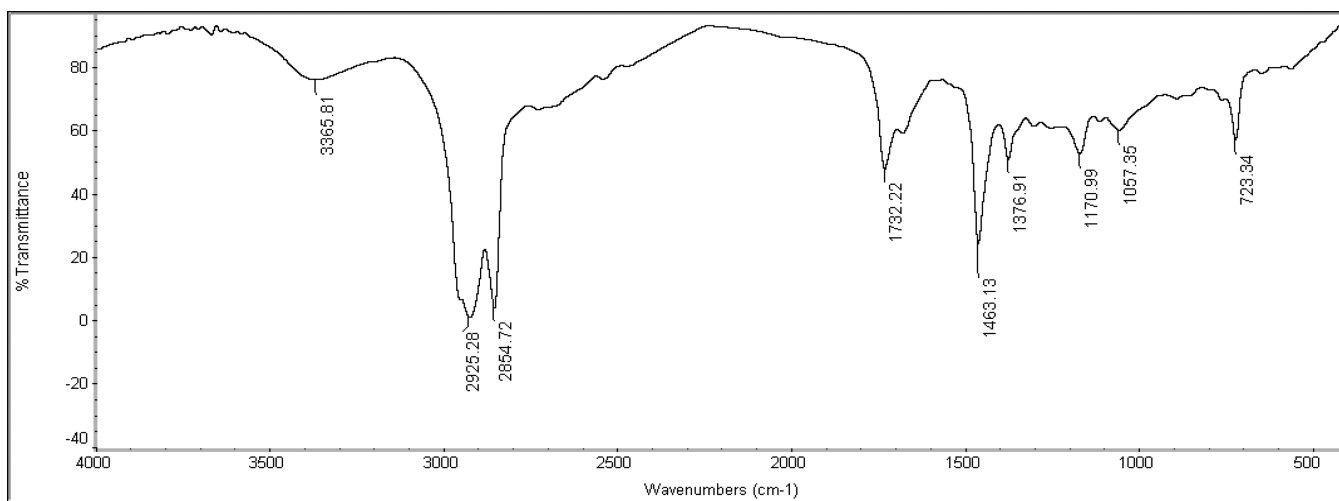
(a)
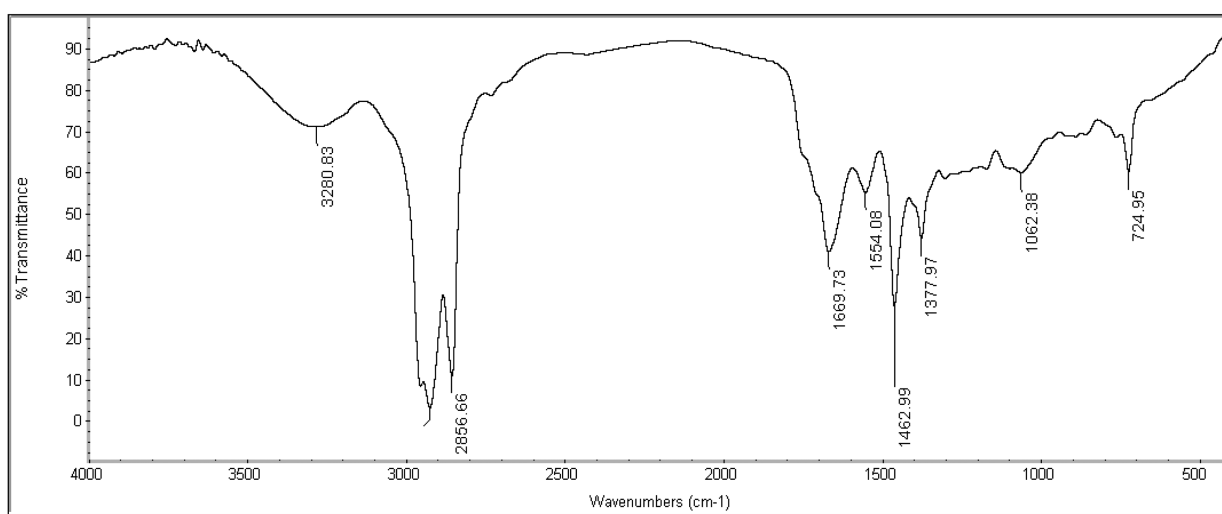
(b)

**Figure 8.** (a, b) FTIR spectrum of the synthesized inhibitors: (a) BTB and (b) DAB.

Scheme 1. This process was carried out using the quaternization reaction. Benzothiazole (50 mM) and 1-bromooctadecane (50 mM) were charged exclusively in a 250 mL round flask with $(CH_3)_2CO$ (100 mL) as a dissolvable solvent. The resulting mixture was refluxed by mixing for 18 h, and then, the resulting mixture was maintained at room temperature. The earthy colored suspension was filtered with a filter paper, washed well twice with diethyl ether, and then recrystallized using $(CH3)_2CO$ to obtain clear product results of the synthesized compounds. The products of the earthy colored precious stone items went somewhere in the range of 78−86%.

The cationic surfactant DAB based on tri-*n*-octyl amine was prepared as illustrated in Scheme 2. This process was carried out using the quaternization reaction. Tri-*n*-octyl amine (50 mM) and 1-bromooctadecane (50 mM) were transferred separately in a 250 mL round flask with $(CH_3)_2CO$ (100 mL) as a dissolvable solvent. The resulting mixture was refluxed by mixing for 18 h, and afterward, the resulting blend was cooled to room temperature. The earthy colored suspension was filtered with a filter paper, washed well twice with diethyl ether,

and afterward recrystallized from $(CH_3)_2CO$ to bear the cost of the white gem results of the cationic surfactants. The products of the earthy colored precious stone items ran somewhere in the range of 80−90%.

3.4.1. Fourier Transform Infrared (FTIR) Spectroscopy Analysis. FTIR spectra of the prepared inhibitors (BTB and DAB) contain two peaks at 3365 and 3280 cm^{-1}, which are ascribed to N−H in both inhibitors, and peaks at 2925 and 2856 cm^{-1} corresponding to CH_3 and CH_2, in addition to a peak at 1057 cm^{-1} and a fingerprint peak at 724 cm^{-1} assigned to the asymmetric and symmetric stretching quaternary nitrogen atom (N^+−C) as shown in Figure 8a,b.

3.4.2. ^1H NMR Spectroscopy. The chemical change at ∂ (1.41) for 1H proton (a) −CH_3, the substance shift ∂ (4.07) for 1H protons (b) −CH_2 related to alkyl collection, this compound shift at ∂ (4.13) for 1H protons (c) −CH_2 of alkyl group alpha. The substance moves between ∂ (8.9) for 1H protons (g) and (h) of aryl ring. All the overhead substance changes affirm that compound BTB was effectively synthesized.
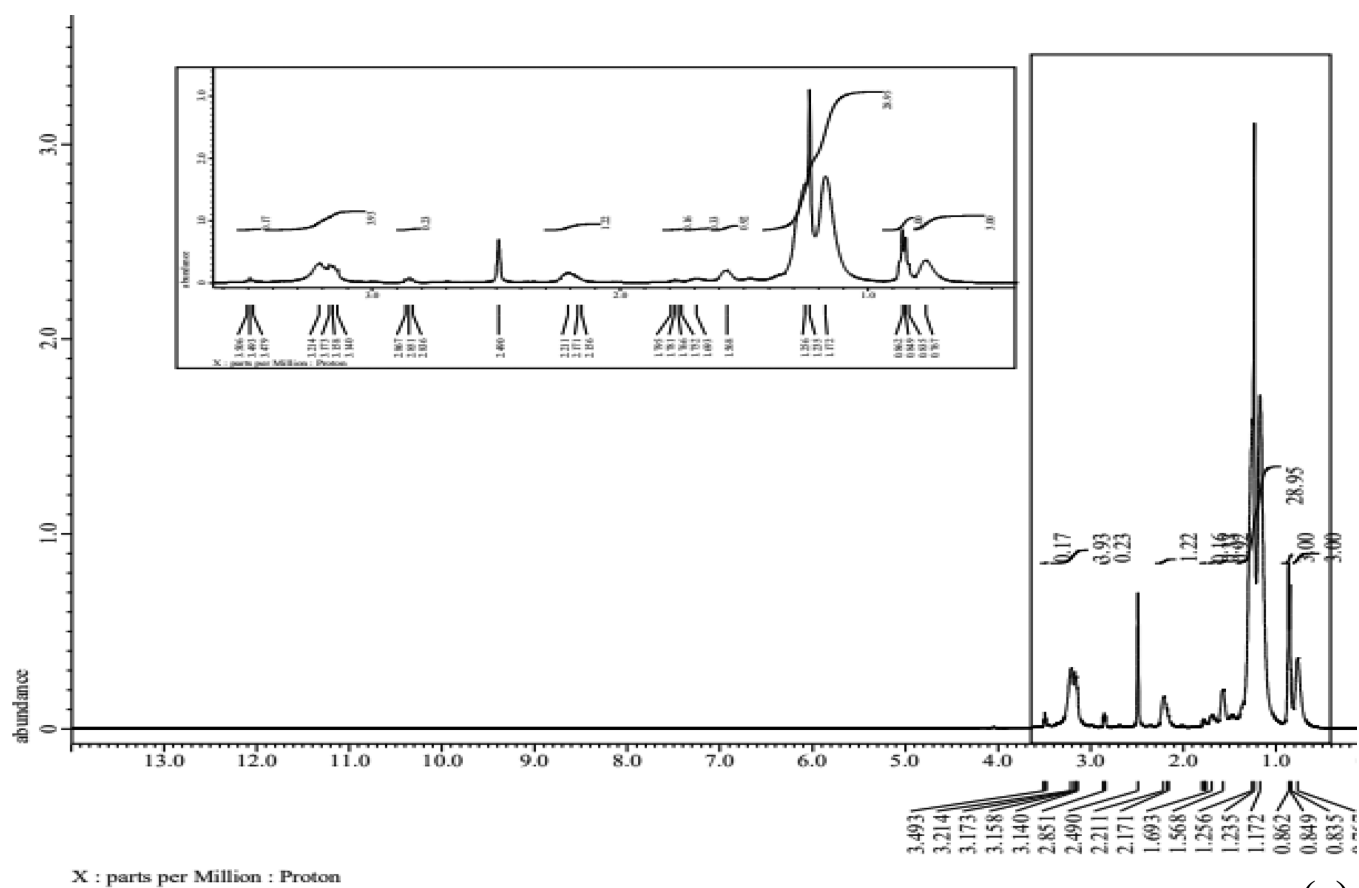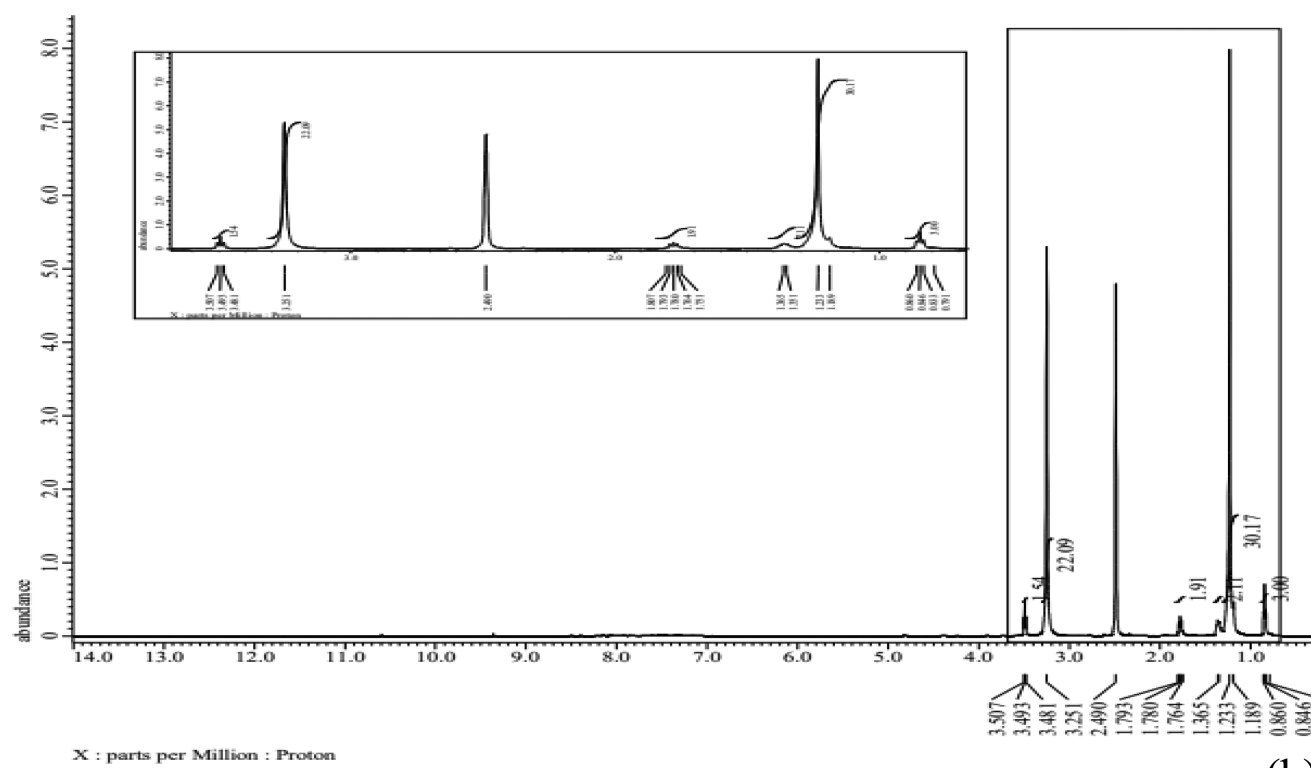
Figure 9. Chemical structure characterization of the inhibitor, (a) ^{1}H-NMR BTB and (b) ^{1}H-NMR DAB.

The chemical shift ∂ (0.88) to 1H proton (a) $-CH_3$, the synthetic ∂ (3.22) for 1H Protons (b) $-CH_2$ related to alkyl group, the compound shift at ∂ (3.28) for 1H Protons (c) $-CH_2$ of alkyl group neer, N−C. inhibitor moves between ∂ (1.26−1.7) for 1H protons (g) and (h) of the alkyl bunch. The above substance shifts confirm that DAB was effectively synthesized. The information of ^{1}H NMR spectra confirmed the normal hydrogen proton dispersion in the combined surfactant as shown in Figure 9a,b.

3.5. Electrochemical Measurements. *3.5.1. Potentiodynamic Polarization Measurement.* Potentiodynamic polarization was carried out in an electrochemical glass cell containing a platinum electrode as an auxiliary electrode and saturated calomel electrode (SCE) as a reference electrode in addition to a working electrode with 1 cm^2 surface area. The used instrument was VoltaLab 80 (Tacussel radiometer PGZ402) with Voltamaster 4 as software for the instrument, and the results were recorded at a scan rate of 1 mVs^{-1} after immersion of the test solution in a three-electrode system for 60 min in the absence and presence of a fixed inhibitor concentration.

3.5.2. Electrochemical Impedance Spectroscopy. Electrochemical impedance spectroscopy (EIS) measurements were carried out in the same electrochemical cell at OCP in the frequency range from 100 kHz to 20 mHz at an amplitude of 10 mV.

3.6. Surface Tension Measurements. The surface tension (γ) was measured using a Krüss K6 tensiometer type, a direct surface tension measurement, using the ring method for various concentrations of the investigated surfactants.

3.7. Surface Examination. In order to record the surface micrographs, the designed samples were immersed in the test solution in the absence and presence of 250 ppm of the inhibitor; after 24 h, the samples were removed from the test solution, cleaned, washed with distilled water, and dried, and the samples were analyzed by AFM conducted using an AFM Nanosurf-Flex-Axiom FlexAFM 5 scan head specifications with a C3000 controller operating in the dynamic force mode at 25 °C.

4. CONCLUSIONS

Newly synthesized surfactants BTB and DAB can be used as effective inhibitors for the dissolution of CS in deep oil well formation water. These surfactants were characterized using FTIR and ^{1}HNMR spectroscopy techniques. The values of the parameters from potentiodynamic polarization measurements of the prepared surfactants show that they act as dual-type inhibitors. AFM micrographs confirm the formation of a good protective film that isolates the surface from the corrosive environment. The synthesized surfactants showed high inhibition efficiency against CS in the formation water.

■ AUTHOR INFORMATION

Corresponding Author

Elsayed Gamal Zaki − *Egyptian Petroleum Research Institute, Nasr City, Cairo 11727, Egypt;* ● orcid.org/0000-0001-7053-3169; Email: chemparadise17@yahoo.com

Authors

Mohamed A. Moselhy − *Belayim Petroleum Company, Cairo 7074, Egypt*

Samir Abd El Hady Abd El-Maksoud − *Chemistry Department, Faculty of Science, Port Said University, Port Said 42522, Egypt*

Mohamed A. Migahed − *Egyptian Petroleum Research Institute, Nasr City, Cairo 11727, Egypt*

Complete contact information is available at:
https://pubs.acs.org/10.1021/acsomega.1c02005

Notes
The authors declare no competing financial interest.

■ REFERENCES

(1) Marín-Cruz, J.; Cabrera-Sierra, R.; Pech-Canul, M. A.; González, I. EIS study on corrosion and scale processes and their inhibition in cooling system media. *Electrochim. Acta* **2006**, *51*, 1847−1854.

(2) Li, X.; Wang, H.; Hu, C.; Yang, M.; Hu, H.; Niu, J. Characteristics of biofilms and iron corrosion scales with ground and surface waters in drinking water distribution systems. *Corros. Sci.* **2015**, *90*, 331−339.

(3) Hernández-Espejel, A.; Domínguez-Crespo, M. A.; Cabrera-Sierra, R.; Rodríguez-Meneses, C.; Arce-Estrada, E. M. Investigations of corrosion films formed on API-X52 pipeline steel in acid sour media. *Corros. Sci.* **2010**, *52*, 2258−2267.

(4) Migahed, M. A.; Al-Sabagh, A. M.; Zaki, E. G.; Mostafa, H. A.; Fouda, A. S. Synthesis of some novel cationic surfactants and evaluation of their performance as corrosion inhibitors for X-65 type carbon steel under H2S environment. *Int. J. Electrochem. Sci.* **2014**, *9*, 7693−7711.

(5) Migahed, M. A.; Zaki, E. G.; Shaban, M. M. Corrosion control in the tubing steel of oil wells during matrix acidizing operations. *RSC Adv.* **2016**, *6*, 71384.

(6) Dickinson, E.; Miller, R. *Food Colloids: Fundamentals of Formulation, Vol 258*. Royal Society of Chemistry, 2001.

(7) Singh, A.; Ansari, K. R.; Quraishi, M. A.; Kaya, S.; Banerjee, P. The effect of an N-heterocyclic compound on corrosion inhibition of J55 steel in sweet corrosive medium. *New J. Chem.* **2019**, *43*, 6303−6313.

(8) Tripathy, D. B.; Murmu, M.; Banerjee, P.; Quraishi, M. A. Palmitic acid based environmentally benign corrosion inhibiting formulation useful during acid cleansing process in MSF desalination plants. *Desalination* **2019**, *472*, No. 114128.

(9) Verma, C.; Haque, J.; Quraishi, M. A.; Ebenso, E. E. Aqueous phase environmental friendly organic corrosion inhibitors derived from one step multicomponent reactions: a review. *J. Mol. Liq.* **2019**, *275*, 18−40.

(10) Cao, C.; Zhang, L.; Zhang, X.-X.; Du, F.-P. Effect of gum arabic on the surface tension and surface dilational rheology of trisiloxane surfactant. *Food Hydrocolloids* **2013**, *30*, 456−462.

(11) Pietralik, Z.; Kołodziejska, Z.; Weiss, M.; Kozak, M. Gemini surfactants based on bis-imidazolium alkoxy derivatives as effective agents for delivery of nucleic acids: A structural and spectroscopic study. *PLoS One* **2015**, *10*, No. e0144373.

(12) Sharma, R.; Kamal, A.; Abdinejad, M.; Mahajan, R. K.; Kraatz, H.-B. Advances in the synthesis, molecular architectures and potential applications of gemini surfactants. *Adv. Colloid Interface Sci.* **2017**, *248*, 35−68.

(13) Nandwani, S. K.; Malek, N. I.; Lad, V. N.; Chakraborty, M.; Gupta, S. Study on interfacial properties of Imidazolium ionic liquids as surfactant and their application in enhanced oil recovery. *Colloids Surf. A Physicochem. Eng. Asp.* **2017**, *516*, 383−393.

(14) Fink, J. K. Drilling muds. In *Pet Eng Guid to oil F Chem fluids*, 2nd ed. Gulf Prof Publ, Published online, 2015, pp. 1−61.

(15) Ziembowicz, F. I.; Bender, C. R.; Frizzo, C. P.; Martins, M. A. P.; de Souza, T. D.; Kloster, C. L.; Santos Garcia, I. T.; Villetti, M. A. Thermodynamic Insights into the Binding of Mono- and Dicationic Imidazolium Surfactant Ionic Liquids with Methylcellulose in the Diluted Regime. *J. Phys. Chem. B* **2017**, *121*, 8385−8398.

(16) Shalabi, K.; Helmy, A. M.; El-Askalany, A. H.; Shahba, M. M. New pyridinium bromide mono-cationic surfactant as corrosion inhibitor for carbon steel during chemical cleaning: Experimental and theoretical studies. *J. Mol. Liq.* **2019**, *293*, No. 111480.

(17) Sengupta, S.; Murmu, M.; Murmu, N. C.; Banerjee, P. Adsorption of redox-active Schiff bases and corrosion inhibiting property for mild steel in 1 molL^{-1} H$_2$SO$_4$: Experimental analysis supported by ab initio DFT, DFTB and molecular dynamics simulation approach. *J. Mol. Liq.* **2021**, *326*, No. 115215.

(18) Hanna, F.; Sherbini, G. M.; Barakat, Y. Commercial fatty acid ethoxylates as corrosion inhibitors for steel in pickling acids. *Br. Corros. J.* **1989**, *24*, 269−272.

(19) Osman, M. M.; Shalaby, M. N. Some ethoxylated fatty acids as corrosion inhibitors for low carbon steel in formation water. *Mater. Chem. Phys.* **2003**, *77*, 261−269.

(20) Al-sabagh, A. M.; Migahed, M. A.; Awad, H. S. Reactivity of polyester aliphatic amine surfactants as corrosion inhibitors for carbon steel in formation water (deep well water). *Corros. Sci.* **2006**, *48*, 813−828.

(21) Abd-Elaal, A. A.; Elbasiony, N. M.; Shaban, S. M.; Zaki, E. G. Studying the corrosion inhibition of some prepared nonionic surfactants based on 3-(4-hydroxyphenyl) propanoic acid and estimating the influence of silver nanoparticles on the surface parameters. *J. Mol. Liq.* **2018**, *249*, 304−317.

(22) Migahed, M. A.; Abd-El-Raouf, M.; Al-Sabagh, A. M.; Abd-El-Bary, H. M. Effectiveness of some non ionic surfactants as corrosion inhibitors for carbon steel pipelines in oil fields. *Electrochim. Acta* **2005**, *50*, 4683−4689.

(23) el-Hajjaji, F.; Messali, M.; Aljuhani, A.; Aouad, M. R.; Hammouti, B.; Belghiti, M. E.; Chauhan, D. S.; Quraishi, M. A. Pyridazinium-based ionic liquids as novel and green corrosion inhibitors of carbon steel in acid medium: electrochemical and molecular dynamics simulation studies. *J. Mol. Liq.* **2018**, *249*, 997−1008.

(24) Qiang, Y.; Zhang, S.; Yan, S.; Zou, X.; Chen, S. Three indazole derivatives as corrosion inhibitors of copper in a neutral chloride solution. *Corros. Sci.* **2017**, *126*, 295−304.

(25) Yilong, Z.; Dean, Z.; Daoliang, L. Electrochemical and other methods for detection and determination of dissolved nitrite: A review. *Int. J. Electrochem. Sci.* **2015**, *10*, 1144−1168.

(26) Tüken, T.; Demir, F.; Kıcır, N.; Sığırcık, G.; Erbil, M. Inhibition effect of 1-ethyl-3-methylimidazolium dicyanamide against steel corrosion. *Corros. Sci.* **2012**, *59*, 110−118.

(27) Sengupta, S.; Murmu, M.; Mandal, S.; Hirani, H.; Banerjee, P. Competitive corrosion inhibition performance of alkyl/acyl substituted 2-(2-hydroxybenzylideneamino) phenol protecting mild steel used in adverse acidic medium: A dual approach analysis using FMOs/molecular dynamics simulation corroborated experimental findings. *Colloids Surf. A Physicochem. Eng. Asp.* **2021**, *617*, No. 126314.

(28) Saha, S. K.; Dutta, A.; Ghosh, P.; Sukul, D.; Banerjee, P. Adsorption and corrosion inhibition effect of schiff base molecules on the mild steel surface in 1 M HCL medium: A combined experimental and theoretical approach. *Phys. Chem. Chem. Phys.* **2015**, *17*, 5679−5690.

(29) Singh, A. K.; Thakur, S.; Pani, B.; Singh, G. Green synthesis and corrosion inhibition study of 2-amino-: N ′-((thiophen-2-yl)-methylene)benzohydrazide. *New J. Chem.* **2018**, *42*, 2113−2124.

(30) Saha, S. K.; Murmu, M.; Murmu, N. C.; Banerjee, P. Evaluating electronic structure of quinazolinone and pyrimidinone molecules for its corrosion inhibition effectiveness on target specific mild steel in the acidic medium: A combined DFT and MD simulation study. *J. Mol. Liq.* **2016**, *224*, 629−638.

(31) Yadav, M.; Kumar, S.; Kumari, N.; Bahadur, I.; Ebenso, E. E. Experimental and theoretical studies on corrosion inhibition effect of synthesized benzothiazole derivatives on mild steel in 15% HCl solution. *Int. J. Electrochem. Sci.* **2015**, *10*, 602−624.

(32) Qiang, Y.; Guo, L.; Li, H.; Lan, X. Fabrication of environmentally friendly Losartan potassium film for corrosion inhibition of mild steel in HCl medium. *Chem. Eng. J.* **2021**, *406*, No. 126863.

(33) Qiang, Y.; Li, H.; Lan, X. Self-assembling anchored film basing on two tetrazole derivatives for application to protect copper in sulfuric acid environment. *J. Mater. Sci. Technol.* **2020**, *52*, 63−71.

(34) Qiang, Y.; Zhang, S.; Tan, B.; Chen, S. Evaluation of Ginkgo leaf extract as an eco-friendly corrosion inhibitor of X70 steel in HCl solution. *Corros. Sci.* **2018**, *133*, 6−16.

(35) Tang, Y.; Yang, X.; Yang, W.; Chen, Y.; Wan, R. Experimental and molecular dynamics studies on corrosion inhibition of mild steel by 2-amino-5-phenyl-1, 3, 4-thiadiazole. *Corros. Sci.* **2010**, *52*, 242−249.

(36) Qiang, Y.; Zhang, S.; Guo, L.; Zheng, X.; Xiang, B.; Chen, S. Experimental and theoretical studies of four allyl imidazolium-based ionic liquids as green inhibitors for copper corrosion in sulfuric acid. *Corros. Sci.* **2017**, *119*, 68−78.

(37) Ashassi-Sorkhabi, H.; Shaabani, B.; Seifzadeh, D. Effect of some pyrimidinic Shciff bases on the corrosion of mild steel in hydrochloric acid solution. *Electrochim. Acta* **2005**, *50*, 3446−3452.

(38) Shaban, S. M. Studying the effect of newly synthesized cationic surfactant on silver nanoparticles formation and their biological activity. *J. Mol. Liq.* **2016**, *216*, 137−145.

(39) Negm, N. A.; Morsy, S. M. I. Corrosion inhibition of triethanolammonium bromide mono-and dibenzoate as cationic inhibitors in an acidic medium. *J. Surfactants Deterg.* **2005**, *8*, 283−287.

(40) Sastri, V. S.; Perumareddi, J. R. Molecular orbital theoretical studies of some organic corrosion inhibitors. *Corrosion* **1997**, *53*, 617−622.